



**HAL**  
open science

## High Frequency Model of Power Transformer Bushing for Very Fast Transient Studies

Anes Messadi, Ayyoub Zouaghi, Esseddik Ferdjallah-Kherkhachi, Christian Vollaire, Olivier Richer, Luiz Fernando de Oliveira, Arnaud Breard

► **To cite this version:**

Anes Messadi, Ayyoub Zouaghi, Esseddik Ferdjallah-Kherkhachi, Christian Vollaire, Olivier Richer, et al.. High Frequency Model of Power Transformer Bushing for Very Fast Transient Studies. *IEEE Access*, 2023, 11, pp.93908-93919. 10.1109/ACCESS.2023.3309702 . hal-04237939

**HAL Id: hal-04237939**

**<https://hal.science/hal-04237939>**

Submitted on 6 Jun 2024

**HAL** is a multi-disciplinary open access archive for the deposit and dissemination of scientific research documents, whether they are published or not. The documents may come from teaching and research institutions in France or abroad, or from public or private research centers.

L'archive ouverte pluridisciplinaire **HAL**, est destinée au dépôt et à la diffusion de documents scientifiques de niveau recherche, publiés ou non, émanant des établissements d'enseignement et de recherche français ou étrangers, des laboratoires publics ou privés.



Distributed under a Creative Commons Attribution - NonCommercial - NoDerivatives 4.0  
International License

Date of publication xxxx 00, 0000, date of current version xxxx 00, 0000.

Digital Object Identifier 10.1109/ACCESS.2017.Doi Number

# High frequency model of power transformer bushing for very fast transient studies

Anes Messadi <sup>1</sup>, Ayyoub Zouaghi <sup>1</sup>, Member, IEEE, Esseddik Ferdjallah-Kherkhachi <sup>2</sup>, Christian Vollaïre <sup>1</sup>, Olivier Richer <sup>2</sup>, Luiz Fernando de Oliveira <sup>3</sup>, Arnaud Breard <sup>1</sup>

<sup>1</sup>Univ Lyon, Ecole Centrale de Lyon, INSA Lyon, Université Lyon 1, CNRS, Ampère, UMR5005, 69130, Ecully, France

<sup>2</sup>R&D dept. Trench France, 68300, Saint Louis, France

<sup>3</sup>R&D dept. WEG, R. Dr. Pedro Zimmermann 6751, Blumenau, Brazil

Corresponding author: A. Zouaghi (ayyoub.zouaghi@ec-lyon.fr).

This work was supported by Trench France.

**ABSTRACT** Fast and very fast transient overvoltages generally appear during switching operations within electrical substations. The oscillatory nature of such phenomena with frequencies that can reach several tens of megahertz tends to degrade the lifetime of high voltage equipment such as bushings and transformers, inducing partial discharges activity or breakdown of the insulation system. According to several case studies, bushings are one of the most sensitive parts to such overvoltages, indeed, a failure in a bushing will in most cases lead to a failure of the transformer, often catastrophically. Generating such overvoltages with a very high frequency character and considerable amplitude can be very difficult, moreover, studying the effect of such overvoltages on the insulated bushings is not easy, even experimentally. Therefore, a simulation of the fast transients in the system can be very useful to understand the consequences of such phenomena. In this context, this document aims to propose a model of high voltage capacitive graded oil impregnated paper (OIP) bushing based on a distributed electrical circuit. The equivalent circuit is constructed based on the geometric design and electrical properties of the materials. The model was developed and implemented using Matlab/Simulink® software, and was validated with experimental measurements based on impedance sweep frequency analysis. The modeling results are in a good agreement with the experimental ones.

**INDEX TERMS** Bushing, distributed circuit model, high voltage, high frequency, impedance analysis, numerical modeling, overvoltage, power transformer, very fast transient.

## I. INTRODUCTION

Bushings play a very important role in the conduction of electrical energy. They ensure the passage of electric current through the walls (structure of a transformer, walls of substations, etc.) as well as the connection between high voltage equipment, such as transformers, generators, Gas Insulated Switchgear (GIS), and the lines of the electrical network [1]–[3]. However, this very essential element in the electrical grid is known to be the most critical and sensitive [4], [5]. A failure can occur either locally or globally, resulting in a complete loss of bushing characteristics. A power transformer can have up to 10 bushings, and the failure of only one of them could induce total transformer failure [5]. In power transformers, the price of a single bushing is only a fraction of that of the transformer. This could lead to the conclusion that diagnosing the condition of the bushings is not economical because they can just be replaced in case of failure. However, about 41% of all high voltage bushing failures result in a transformer fire or

explosion [5]–[7]. A bushing failure can damage a transformer in different ways. It has been found that the explosion of the upper porcelain insulator ejects fragments at tremendous speeds which possess a destructive effect. In addition, the bursting of the lower part modifies the internal dielectric characteristics of the transformer due to the burns and waste which pollute its active part [8]. Because of the fact that the oil inside the transformer is not static, the metal debris due to the explosion of the internal electrodes can be easily transported relatively far from the point of impact thus causing other damage such as the rupture of insulation or partial discharges [9], [10].

It is known that all the high voltage equipment that makes up the substations are exposed to overvoltages of different forms. According to the IEC standard [11], these transient overvoltages are classified into three categories: Slow-front overvoltages usually caused by the commissioning and energizing of transformers, Fast-front overvoltages often

referred to as lightning surge and finally Very fast front overvoltages (VFTO: Very Fast Transient Overvoltage) which frequently appear during the switching operations of the disconnectors inside the GIS substations [12]–[14]. This last category is distinguished by its very low rise time of the order of 4 to 100 ns and is not yet covered by conventional acceptance tests. The bushings are the most sensitive parts during VFTO events due to their very compact and fragile structure [15], [16]. Faced with such a phenomenon, the distribution of the potential inside the capacitive body of the bushing becomes non-uniform, thus causing discharges which gradually degrade its internal insulation [10], [17]. Transients can also be responsible for disturbance of control command and communication circuits at weak currents by conduction or electromagnetic radiation, a drop in continuity of service and a danger to the safety of people.

The impact of very fast transients on bushings has been observed for a long time, however, with the development of electrical network architectures and the tendency to integrate intermittent renewable energies and power electronic converters, the energy network becomes more complex and generates, consequently, more frequent operation of switching systems, which increases the likelihood of having very severe transients [3], [18]–[20].

These phenomena of non-standard transient overvoltages rise a lot of concern to ensure the performance of high voltage systems over the long term, and to understand the behavior and the constraints that these bushings can undergo under such high frequency waves. Carrying out such a study experimentally can be very difficult and complicated especially if it is a question of generating such very high amplitude overvoltages with a frequency character of the range of several tens of megahertz. Developing a high frequency model capable of simulating the bushing behavior under fast transients is a fundamental step to understand these phenomena and their consequences on the bushings and the transformers. This model must be able to give the same frequency response as that of the bushing under fast transient overvoltages.

In the literature, the works dealing with bushing modeling in high frequencies are so few. The choice of modeling approach is a crucial step to get accurate results. The finite element method is one of the modeling approaches that can be used to study the electric field distribution in bushing under transient [21]. It makes it possible to have the electric field distribution in the bushing under different electrical and thermal conditions [16], [22]. Despite its high accuracy, it has a very high computation time especially when dealing with a complex system, high frequency and iterative computations [23]. Moreover, the knowledge of the internal design and the dimensions of each part of the bushing is necessary for the modeling part, because numerical modelling such as FE method and analytical formulas are based on geometrical dimensions and the materials properties. In this work, a distributed electrical circuit model

has been carried out [16]. This model has several advantages such as reduced computation time and high accuracy [12]. It allows access to the electrical quantities such as voltage and current in each part and each layer of the bushing. Electric circuit based modeling approach has been employed efficiently for transformers modeling [24], [25]. However, this modeling approach based on electric circuits with lumped constants remains valid if the device remains small compared to the minimum wavelength of the maximum study frequency. That's why a distributed version of the equivalent circuit model is used in this paper due to the size of the studied device. To achieve such a model, several study steps have been accomplished, they have been structured into three main sections: sweep frequency impedance analysis section where the experimental setup and protocols are described, bushing modeling section where the different steps for the circuit elements parameters determination and their frequency validity are presented, and results and discussion section where the results of both experimental and modeling studies are presented and discussed.

## II. SWEEP FREQUENCY IMPEDANCE ANALYSIS

To validate a model, it is necessary to compare its response with the experimental response of the bushing. For the experimental study, the sweep frequency impedance analysis [26]–[29], which consists of measuring the impedance of the bushing over a wide range of frequencies, has been carried out in this work. This technique is considered as an efficient non-intrusive tool for fault diagnosis in transformers and their accessories.

### A. EXPERIMENTAL SETUP

The bushing under investigation is characterized by a nominal voltage of  $U_n = 145$  kV, and a nominal current  $I_n = 2$  kA (Figure 1). Its active part (internal part) is based on oil impregnated paper (OIP) capacitive grading technology, with 41 aluminum conductive layers. The bushing was installed horizontally in a wooden box insulated from the ground and in a suitable position while leaving the central conductor as well as the test tap accessible for measurement. To perform the measurements, a high-resolution KEYSIGHT AGILENT HP 4294A impedance analyzer with a bandwidth ranging from 40 Hz to 110 MHz was used. The analyzer is equipped with a measurement probe which offers the possibility of performing measurements with high precision. An impedance calibration kit is also used, essentially comprising open circuit, short circuit and  $50 \Omega$  load standards. The purpose of the calibration is to compensate some disturbances generated by the measurement cables and which appear at high frequency. To confirm the status or accuracy of the calibration, a  $25 \Omega$  resistive load is used, this impedance value was not used during the calibration phase.

The objective of the experimental setup is to characterize the impedance of the bushing as a function of the frequency for three test configurations which are presented in Figure 1.

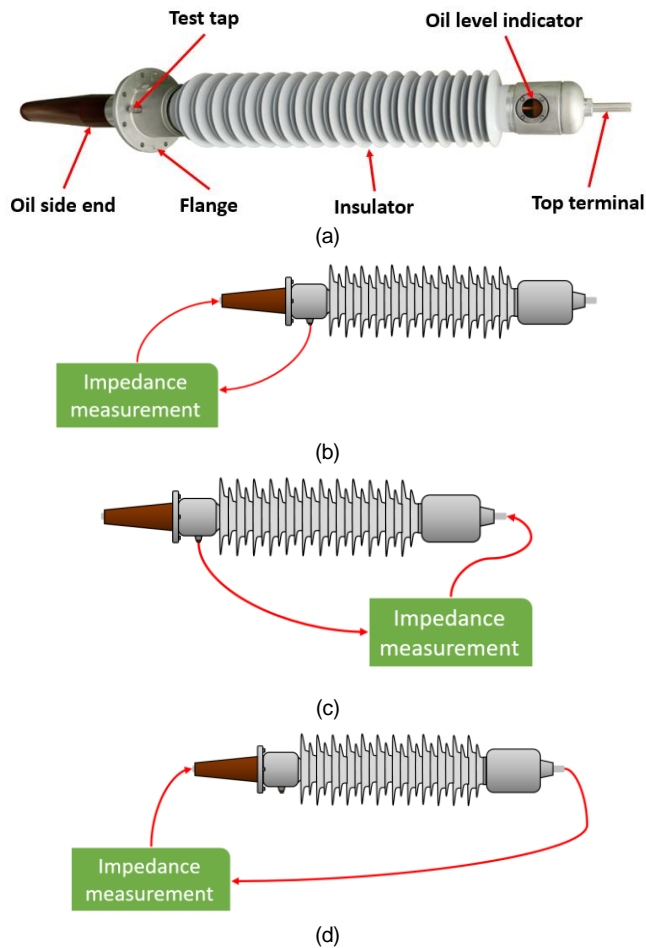


**FIGURE 1.** Experimental configurations for impedance analysis. (a) Bushing image. (b) Configuration 1: Impedance analysis between the central conductor and the test tap on the lower side of the bushing (Transformer side). (c) Configuration 2: Impedance analysis between the central conductor and the test tap on the upper side (Line side). (d) Configuration 3: Impedance analysis between the terminals of the center conductor with the test tap connected to the ground.

In the first configuration, the impedance is measured between the central conductor and the test tap on the lower side of the bushing (transformer side). In the second configuration, the measurement is made also between the central conductor and the measurement tap, but on the upper side of the bushing (line side). In the third configuration, the impedance is measured between the central conductor terminals with the test tap isolated from the ground. For this third configuration, preliminary measurements have shown that the connection of the test tap to the ground does not affect considerably the frequency response.

### B. MEASUREMENT PROTOCOL

For accurate measurements, an experimental protocol of several steps was followed:

1) Adjustment and configuration of the impedance analyzer by choosing the number of data to be collected (in our case, the choice was made on 801 points.), initial and final frequency of the Sweep as well as the logarithmic display scale.

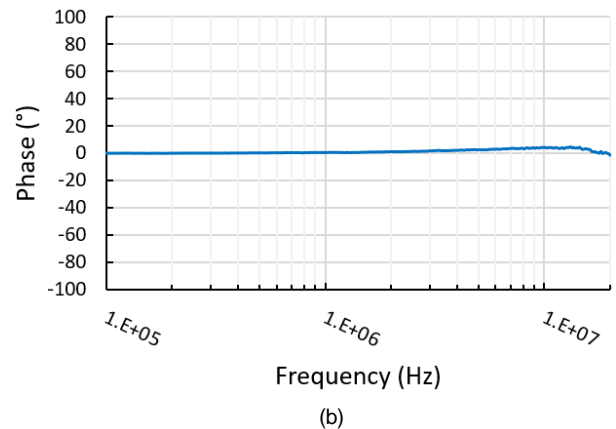
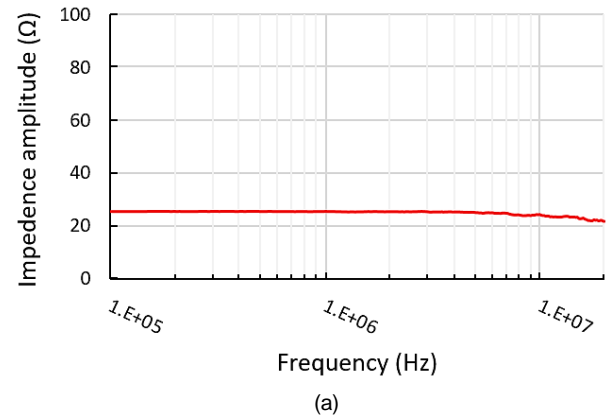


**FIGURE 2.** Results of impedance measurement of 25  $\Omega$  resistor after the calibration over a wide range of frequency up to 20 MHz, (a) the amplitude, (b) the phase.

- 2) A calibration process is carried out (open circuit, short circuit, and load) for each measurement configuration due to the length of the wires which changes for each test.
- 3) Verification of the calibration quality with the minimum loss resistor of 25  $\Omega$ .
- 4) Make the connection on the bushing and start the measurement of the impedance spectrum and save the data.
- 6) Repeat the same steps for each measurement configuration shown in Figure 1.

It should be noted that the maximum studied frequency is 20 MHz. The compensation of all the disturbances for frequencies higher than 20 MHz was not possible. The results of the measurements of the minimum loss resistor of 25  $\Omega$  after the calibration is illustrated in Figure 2. One can see that the perturbations have been successfully compensated and eliminated over the entire frequency range.

### III. BUSHING MODELING

In this work, a distributed electric circuit method is used because of its simplicity, and its proved applicability for modeling several electrical systems such as power transformers [24], transmission lines [30], etc. In this section, the analytical equations allowing the calculation of R, L and C elements of the equivalent circuit will be presented and validated by finite element simulation on COMSOL

Multiphysics®. The simulation aims to identify in which frequency range the analytical equations are valid. The equivalent circuit is implemented on Matlab/Simulink® and will be subjected to impedance analysis tests to extract its signature, which will be compared with the results of the experimental study.

### A. DISTRIBUTED CIRCUIT MODEL

The distributed element model assumes that the circuit elements (resistance, capacitance, and inductance) are continuously distributed throughout the circuit material of the system to be modeled. In the distributed element model, each element of the circuit is infinitely small. Such a model assumes a non-uniform current along each branch and a non-uniform voltage along each wire. The distributed model is used where the wavelength becomes comparable to the physical dimensions of the circuit. This occurs at high frequencies, where the wavelength is very short [31].

The knowledge of the internal design and the dimensions of each part of the bushing is necessary for the modeling part, because all the analytical formulas are based on geometrical dimensions and the materials properties. The active part of the bushing under investigation is made up of multiple aluminum layers arranged in a staircase in the upper and lower part of the bushing. The last layer is connected to the test tap. These layers are isolated from each other by OIP ( $\epsilon_r = 4.2$ ). This arrangement of the layers makes it possible to better control both radial and axial distribution of the electric field, and keep it within the design rules limits. Figure 3 shows a simplified cross-sectional diagram of the bushing, and its equivalent circuit. The conductive parts such as the central conductor and the aluminum layers are modeled by an R-L series equivalent circuits. The dielectric parts are modeled using R-C parallel equivalent circuit at the early stage, then an equivalent series resistance has been added in order to improve the model at high frequencies (Figure 3.b). The circuit elements equations are described in the next section.

### B. ANALYTICAL EQUATIONS

In the following, the elementary circuit parameters per unit length R, L, G and C of a coaxial line will be described.

#### Capacitance and leakage conductance of insulating material:

The capacitance per unit length in F/m and the conductance per unit length in S/m of an insulating material in coaxial geometry (which corresponds to a crossing section of the bushing with a single sheet) with the central conductor having radius  $a$  and the outer conductor having radius  $b$ , can be expressed by the equations:

$$C = \frac{2\pi\epsilon}{\ln(b/a)} \quad (1)$$

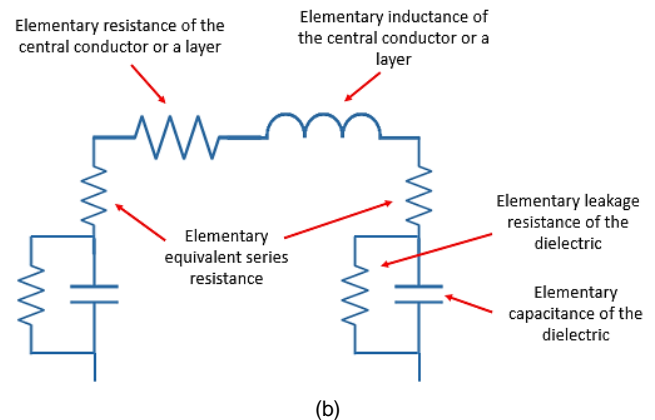
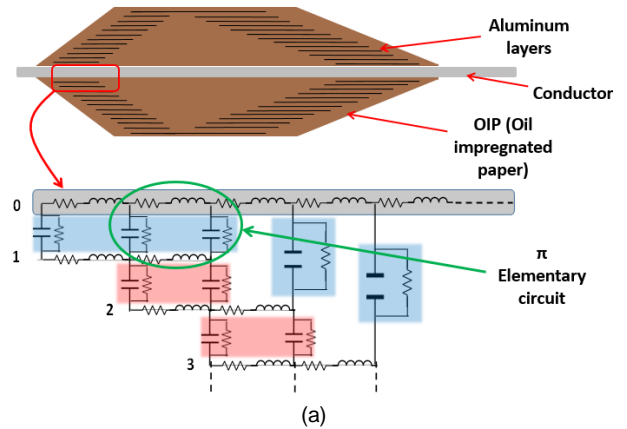


**FIGURE 3.** (a) Cross-sectional layout of the bushing, and its equivalent circuit. The blue segments are referring to the dielectric insulation between the aluminum sheets and the central conductor. The red segments are referring to the dielectric insulation between the aluminum sheets. (b) One single element of the equivalent circuit.

$$G = \frac{2\pi\sigma}{\ln(b/a)} \quad (2)$$

Where,  $\epsilon$  and  $\sigma$  are the permittivity and the electrical conductivity of the insulating material respectively.

For a bushing composed of multiple layers, the linear capacitance and conductance between two successive layers can be expressed respectively as:

$$C(i) = \frac{2\pi\epsilon}{\ln(D(i+1)/D(i))} \quad (3)$$

$$G(i) = \frac{2\pi\sigma}{\ln(D(i+1)/D(i))} \quad (4)$$

Where,  $i = 0, 1, \dots, n$  is the layer number.  $i = 0$  for the inner conductor.  $D(i)$  is the inner diameter of the layer number  $i$ .

#### Inductance and resistance of conducting material:

The inductance per unit length of the central conductor (in H/m) with a magnetic permeability  $\mu$  in a coaxial configuration is described by the equation:

$$L_c = \int_a^b \left( \frac{\mu}{2\pi r} \right) \cdot dr = \frac{\mu}{2\pi} \cdot \ln \left( \frac{b}{a} \right) \quad (5)$$

With  $a$  being the outer radius of the central conductor, and  $b$  the inner radius of the outer conductor. This equation is generally referred to as the coaxial cable high frequency inductance. For the aluminum sheets, the current sheet theory can be used, the equation (6) suggested by [32] is employed to calculate the self-inductance:

$$L_{\text{layer}} = \mu A / h \quad (6)$$

$A$  represents the cross-sectional area of the sheet, and  $h$  its length.

The resistance per unit length of the central conductor which has a cylindrical shape can be expressed as follows:

$$R_c = \frac{1}{\sigma \cdot S} \quad (7)$$

With  $S$  being the section of the conductor and  $\sigma$  its electrical conductivity.

The equation (8) presents the inherent resistance per unit length of each cylindrical aluminum sheet considering the internal and the external radiuses,  $b$  and  $b'$  respectively of the layer:

$$R_{\text{layer}} = \frac{1}{\pi \sigma (b'^2 - b^2)} \quad (8)$$

Before establishing the high frequency circuit model, it is necessary to ensure in which frequency range the equations determined previously are valid. Due to the non-linear behavior in high frequencies, the behavior of the equivalent electric circuit can be very complex, this non-linearity is translated by the frequency dependence of the parameters of the circuit. In the following, finite element simulations of a crossing section have been carried out on COMSOL Multiphysics® to study the frequency behavior of each element of the circuit.

### C. NUMERICAL SIMULATION

To determine the properties of the inductive and the insulating materials, an electromagnetic study was carried out on COMSOL Multiphysics® for a 2D geometry which represents an elementary section of a crossing Figure 4.

To simulate the bushing conductive parts, five circles were designed in COMSOL Multiphysics® with radiuses of 40, 41, 41.2, 42 and 42.2 mm. This geometry consists of a central conductor and two concentric aluminum sheets. The conductive parts are defined as Coils (single-turn coil in COMSOL Multiphysics®), to be able to excite them using

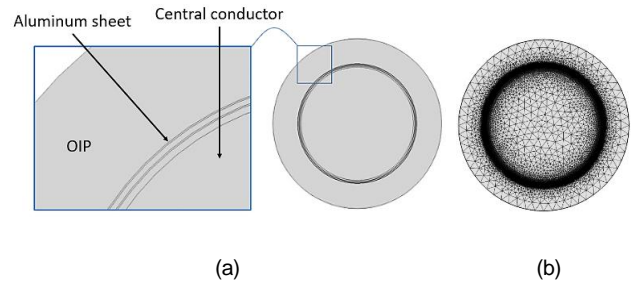


FIGURE 4. Cross-sectional geometry of the bushing (a) without and (b) with a mesh.

TABLE I  
THE PHYSICS USED FOR FINITE ELEMENT MODELING AS WELL AS THE ASSOCIATED EQUATIONS.

Physic	Equations
Magnetic and electric fields module	$\nabla \times \mathbf{H} = \mathbf{J}$ $\mathbf{B} = \nabla \times \mathbf{A}$ $\mathbf{E} = -\nabla V - j\omega \mathbf{A}$
Electrostatics module	$\nabla \cdot \mathbf{D} = \rho$ $\mathbf{E} = -\nabla V$

an electric current. The length of the system along the  $z$  axis is fixed at 864 mm. Aluminum was used as conductive material in both central conductor and the sheets with a conductivity value per unit length of  $36.9 \cdot 10^6$  S/m and relative permeability of 1. Oil impregnated paper is considered as insulating material with a lineic conductivity of  $6.3 \cdot 10^{-11}$  S/m and a relative permittivity of 4.2. The mesh adaptation is an essential step to get accurate results. In our case, a triangular mesh has been chosen, it is important to ensure that the mesh is refined enough at the interfaces. The meshed geometry is illustrated in Figure 4.b. The used mesh is composed of 32420 elements, with a size ranging between 200  $\mu\text{m}$  and 5 mm, depending on the region.

To solve such a finite element model in frequency domain, two physics were used in COMSOL, "magnetic and electric fields" and "electrostatics", which allow the solution of Maxwell equations summarized in the Table I. In these equations,  $\mathbf{H}$  represents the magnetic field,  $\mathbf{E}$ : the electric field,  $\mathbf{D}$ : displacement field,  $\mathbf{B}$ : magnetic induction,  $\mathbf{A}$ : magnetic potential vector,  $V$ : the electric potential,  $\mathbf{J}$ : current density,  $\rho$ : the space charge which is neglected in this simulation.

#### Inductances:

By solving the above equations, the inductance of the conductive parts has been determined using the energy method based on the total magnetic energy of the system. The equation can be defined as [34], [35]:

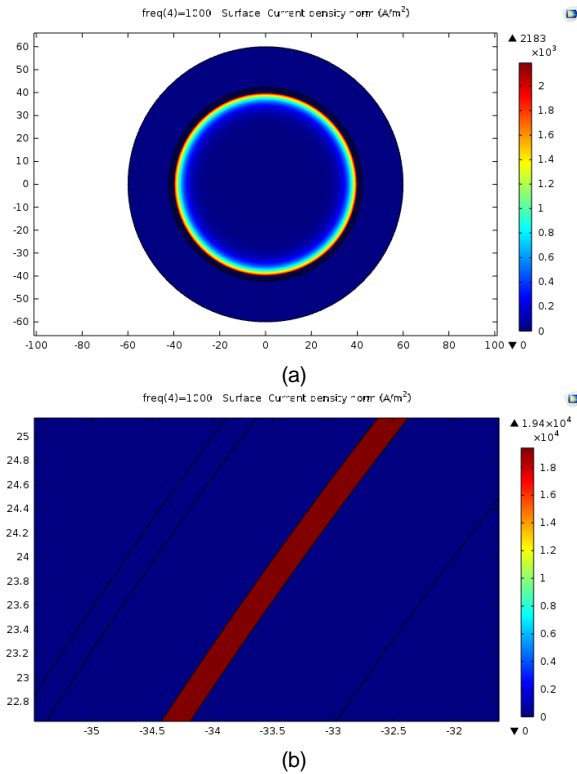


**FIGURE 5.** Illustration of the skin effect. (a) Distribution of the current density in the central conductor for a frequency of 1000 Hz. (b) Distribution of the current density in one aluminum sheet for a frequency of 1000 Hz.

$$L = \frac{2}{I^2} \int W_m \, d\Omega \quad (9)$$

Where  $W_m$  being the magnetic energy density determined from an integrated function in COMSOL Multiphysics®.  $I$  is the current crossing the conductive part which equals to 1 A.

The variation of inductance of the central inductor and the first aluminum sheet in a frequency range from 1 to  $10^8$  Hz is listed in the Table II. One can notice that the inductance value of the central conductor decreases as a function of the frequency then it stabilizes at high frequencies. The analytical calculation of the inductance using the equation (5) with  $b = 41$  mm,  $a = 40$  mm and  $l = 864$  mm give an equal value of  $4.2669 \times 10^{-9}$  H. This value, according to simulation results presented in Table II, is not valid in the frequency range from 1 to  $10^5$  Hz, nevertheless it is close to numerical values for frequencies higher than  $10^5$  Hz. This means that the equation (5) which will be used in the model is guaranteed only at high frequencies. This observation has also been affirmed in the literature [36].

The same approach was applied for the aluminum layers. By applying a current of 1 A, the inductance of the first layer was calculated for different frequency values (See Table II). These results show that the value of the inductance is almost constant up to  $10^6$  Hz, then it decreases for higher frequencies. This inductance was also calculated analytically using the same equation (5). The result of the calculation showed that this equation is not accurate for the aluminum layer. However,

**TABLE II**  
SELF-INDUCTANCE OF THE CENTRAL CONDUCTOR AND THE FIRST ALUMINUM SHEET AS A FUNCTION OF THE FREQUENCY

Frequency [Hz]	Central conductor inductance [H]	Aluminum sheet inductance [H]
1	4.7442E-8	7.0073E-11
50	2.9119E-8	7.0073E-11
100	2.1983E-8	7.0073E-11
1000	9.9212E-9	7.0073E-11
10000	6.0578E-9	7.0073E-11
1E5	4.8248E-9	7.0047E-11
1E6	4.3134E-9	6.7525E-11
1E7	4.2674E-9	1.4682E-11
1E8	4.2669E-9	1.8525E-13

using the equation (6), the inductance of the first layer gives a value of  $7.51 \times 10^{-11}$  H. This value is a little bit higher than but in the same order of magnitude of the numerical values obtained using COMSOL Multiphysics® for frequencies lower than  $10^6$  Hz. It is observed that the used equations for the central conductor and the sheets are valid at different frequency ranges. The equation used for the sheets underestimates the inductance values for frequencies higher than 1 MHz. This can be explained by the fact that both equations do not consider the frequency effect. The assumption of not considering the frequency effect has been made in this work in order to simplify the problem. The complexity of the busing geometry and the interactions between the conductive layers makes it very difficult to get an accurate analytical equation for the inductance in a wide frequency range.

### Resistances:

The electromagnetic simulations carried out previously make it possible also to calculate the resistances of the central conductor and the aluminum layers. Theoretically, this resistance varies considerably with frequency due to the skin effect. The results of the frequency domain study on COMSOL Multiphysics® confirm this as shown in Figure 5.a in which the skin effect is clearly visible through the surface distribution of the current density in the central conductor.

Table III presents the resistance values obtained using numerical simulation for the central conductor and the first aluminum sheet. Modeling the skin effect endowed with a non-linear resistance behavior by an electrical circuit is very difficult. That said, for a first step, an assumption was made, neglecting the skin effect. Therefore, we have used the classic analytical equation (7) which is valid only at very low frequency and which gives a value of  $4.66 \times 10^{-6} \Omega$ .

The same numerical study has been applied to the aluminum layers except that the thickness of the latter is of the order of a micrometer. The skin effect in this case is almost negligible, this can be seen through the density distribution of current illustrated in Figure 5.b. The numerical calculated resistance values of the first aluminum layer are presented in the third column of Table III, one can see that the resistance is nearly

TABLE III  
NUMERICAL CALCULATION OF THE RESISTANCE OF THE CENTRAL CONDUCTOR AND THE FIRST ALUMINUM SHEET AS A FUNCTION OF THE FREQUENCY

Frequency [Hz]	Central conductor resistance [ $\Omega$ ]	Aluminum sheet resistance [ $\Omega$ ]
1	4.6635E-6	4.5335E-4
50	9.2293E-6	4.5335E-4
100	1.2497E-5	4.5335E-4
1000	3.6751E-5	4.5335E-4
10000	1.1373E-4	4.5336E-4
1E5	3.8881E-4	4.5421E-4
1E6	0.0011461	5.3576E-4
1E7	0.0012583	0.0022452
1E8	0.0012597	0.0027141

constant between 1 and  $10^5$  Hz. The analytical equation (8) was used to calculate the inherent resistance of the first layer and it gives a resistance value of  $4.53 \times 10^{-4} \Omega$ .

### Capacitances:

To study the variation of the capacitance of the dielectric (oil impregnated paper) as a function of the frequency, an electrostatic frequency domain study was carried out in COMSOL Multiphysics®.

Let's take as an example the dielectric located between the central conductor and the first layer. To calculate this capacitance (denoted  $C_1$ ), one of the conductors is put under voltage of 1 V while the other is put at zero potential. This allows to apply the energy method based on the total electrical energy density of the system defined by the equation (10) to deduce the value of the capacitance  $C_1$ :

$$C_1 = \frac{2}{V^2} \int E_e \, d\Omega \quad (10)$$

Where,  $E_e$  is the electric energy density determined from an integrated function in COMSOL Multiphysics®.  $V$  is the applied voltage which equals to 1 V.

The same approach is applied to calculate the capacitance  $C_2$  of the dielectric between the first and the second layer. As the Electrostatic module was used to model the capacitances and none non-linear behavior was taken into account, the results show that the capacitances  $C_1$  and  $C_2$  are constant and their values are  $8.17 \times 10^{-9}$  F and  $1.05 \times 10^{-8}$  F respectively. The calculation of these capacitances by the analytical equation (3) gives the same results.

This finite element simulation allowed us to verify the analytical equations and evaluate their accuracy over a wide range of frequency. Indeed, it has been found that each analytical equation is only valid over a very specific frequency range, for example, the calculation of the resistances has shown that it is only valid at low frequencies. In fact, the analytical equations don't consider the frequency effect. Making such assumptions simplifies the study in terms of the complexity of the electrical circuit and simulation time. However, these assumptions can also have negative

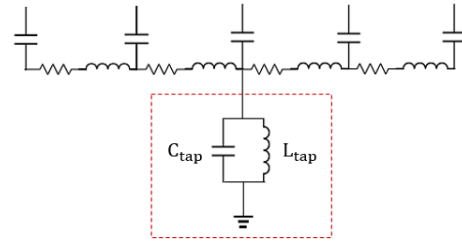


FIGURE 6. Electrical model of the test tap outlet added to the previous model.

consequences on the accuracy of the model. In this work, we will be satisfied with these equations for the calculation of the elements of the equivalent circuit. However, to get a more accurate model, the frequency effect should be considered.

Once these equations have been validated, the next task is to build up the model of the bushing based on the elementary electrical circuit.

### D. MODEL IMPROVEMENT ELEMENTS

The results of the first modeling, which will be presented in the next section, were not satisfactory in high frequencies, so these model improvements have been made.

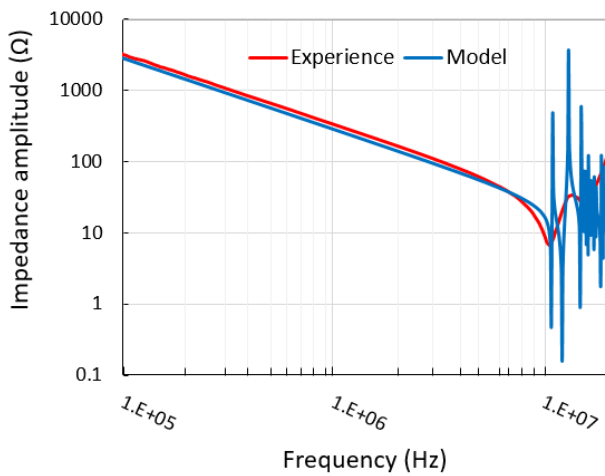
To improve this model, an equivalent electrical circuit of the test tap which is connected to the last aluminum layer is considered. The test tap is essentially composed of a small multi-strand wire welded to the last aluminum sheet, this means that it can be modeled by a simple inductance  $L_{tap}$ . On the other hand, a parallel capacitance  $C_{tap}$  is also considered in this model which represents the capacitance between the grounded layer and the flange as shown in Figure 6. The calculation of these quantities was made approximatively, their values are 0.1  $\mu$ H and 0.65 nF for the tap inductance and the capacitance respectively.

On the other hand, a modification has been made in the elementary circuit of the dielectric material by adding an equivalent series resistance (ESR) [37], [38]. This series resistive element represents the energy losses through the heating generated by current. It depends on the type of the dielectric material and the electrodes; it is related to the dissipation factor of the dielectric. In other words, there is an expression that relates this dissipation factor ( $\tan \delta$ ) with the capacitance of the dielectric and the ESR [39], and can be calculated using the equation :

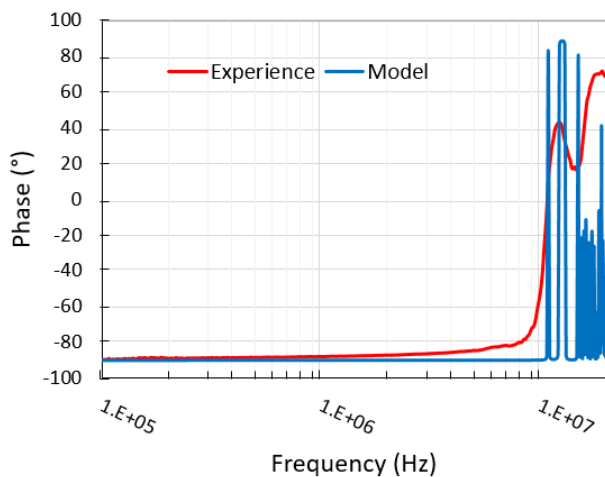
$$\tan \delta = \frac{ESR}{|Z_c|} \quad (11)$$

By knowing  $\tan \delta$  and the impedance  $Z_c$  one can determine the value of the ESR, however the dissipation factor is frequency dependent, and the manufacturer provides it only at industrial frequency (equal to  $2.4 \times 10^{-3}$  at industrial frequency 50 Hz). To determine the ESR in this case, we will directly use the first two impedance measurements (measurements 1 and 2) on which we can extract the value of the impedance which corresponds to the natural resonance frequency (10 MHz in our bushing), this value corresponds to the series equivalent resistance of the entire bushing  $ESR_T$ . Knowing that the





(a)



(b)

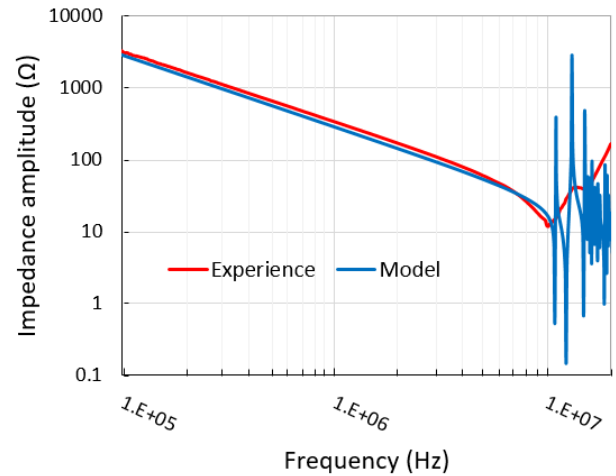
**FIGURE 6.** Impedance frequency analysis of the bushing using the configuration 1, without improvement elements. Model results in blue and experimental results in red. (a) amplitude measurement, (b) phase measurement.

crossing has 41 layers and each layer contains an ESR, then dividing  $ESR_T$  by 41 will therefore give the value of the resistance for one layer. The accuracy of this simplified approach can be questioned, however, the simulation results have shown a remarkable improvement when ESR has been added at each layer, the results are presented in the next section.

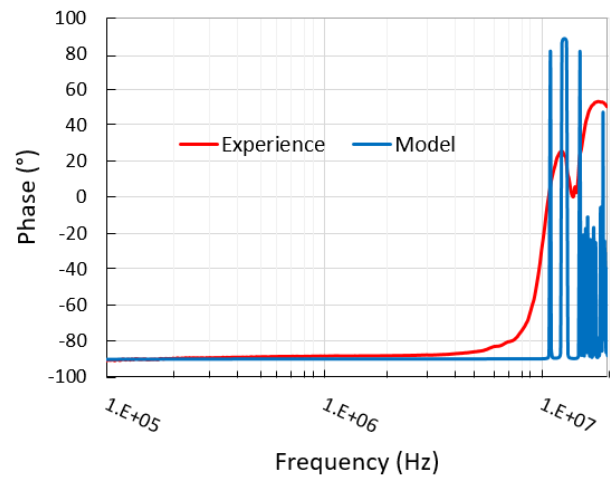
In addition to the test tap circuit elements and the ESR, an inductive element with a suitable estimated value has been added in series of the circuit in order to compensate additional inductive components of the measurement cables and the central conductor terminations.

#### IV. RESULTS AND DISCUSSION

In this section, the results of the impedance analysis of the bushing circuit model are analyzed and compared with the



(a)



(b)

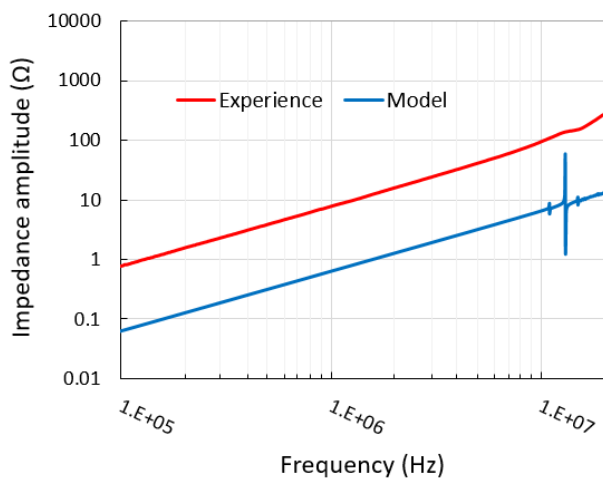
**FIGURE 7.** Impedance frequency analysis of the bushing using the configuration 2, without improvement elements. Model results in blue and experimental results in red. (a) amplitude measurement, (b) phase measurement.

experimental results. The simulation has been carried out using Matlab/Simulink®, on the same configurations studied experimentally, with frequencies ranging from 0.1 to 20MHz. The results of the model excluding the improvement elements are presented firstly, then the results of the model including the improvement elements.

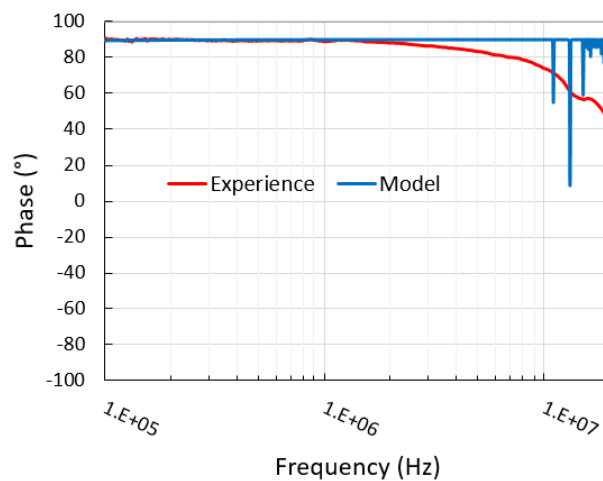
#### A. RESULTS WITHOUT MODEL IMPROVEMENT ELEMENTS

The simulation and experimental results of the amplitude and the phase are presented in Figures 6, 7 and 8 for the 3 configurations 1, 2 and 3 (check Figure 1) respectively.

It can be seen from Figures 6, 7 that the curves from the model and the experiments are almost superimposed between 0.1 and 8 MHz with a pure capacitive behavior in terms of amplitude and a phase of  $-90^\circ$ . However, when the frequency reaches 8 MHz, the model results diverges from



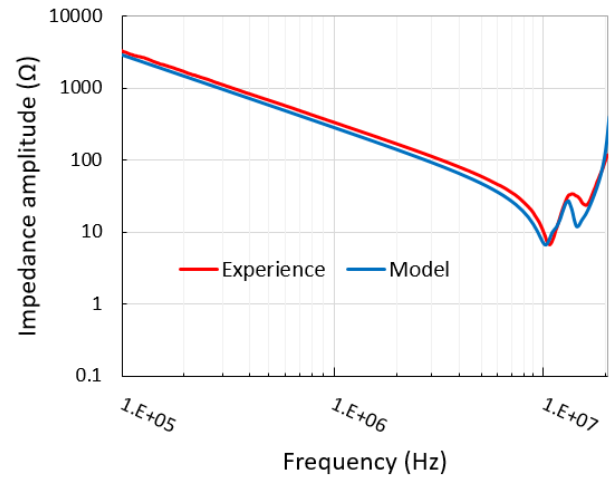
(a)



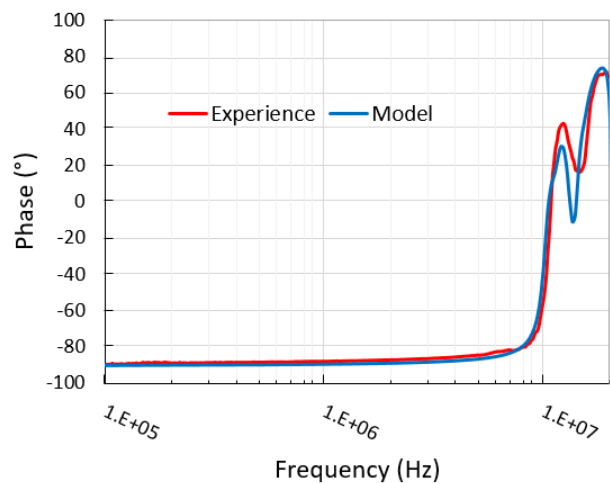
(b)

**FIGURE 8.** Impedance frequency analysis of the bushing using the configuration 3, without improvement elements. Model results in blue and experimental results in red. (a) amplitude measurement, (b) phase measurement.

the measurements with the appearance of several resonances and antiresonances of high amplitude at frequencies higher than 10 MHz. These deviations can be attributed to high frequency response of the equivalent circuit and the simplification assumptions considered. The responses obtained for the 3rd configuration (Figure 8) represent an inductive behavior with a phase equal to  $90^\circ$ , with the presence of some resonances for frequencies higher than 10 MHz. Indeed, a difference of amplitude is observable between the model (blue curve) and the experimental results (red curve). The difference value depends on the frequency, it is smaller at low frequencies and larger at high frequencies. This may be due to the assumption that was taken into account in the modeling of the central conductor with a circuit R-L series which does not take skins effect into consideration. Neglecting such a nonlinear phenomenon could significantly affect the frequency response of the



(a)



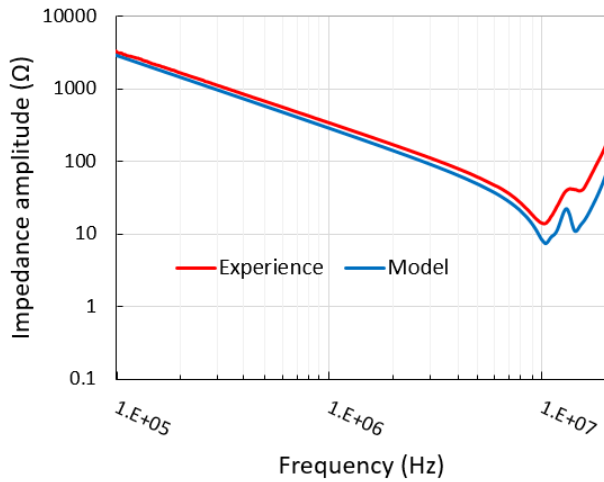
(b)

**FIGURE 9.** Impedance frequency analysis of the bushing using the configuration 1, with improvement elements. Model results in blue and experimental results in red. (a) amplitude measurement, (b) phase measurement.

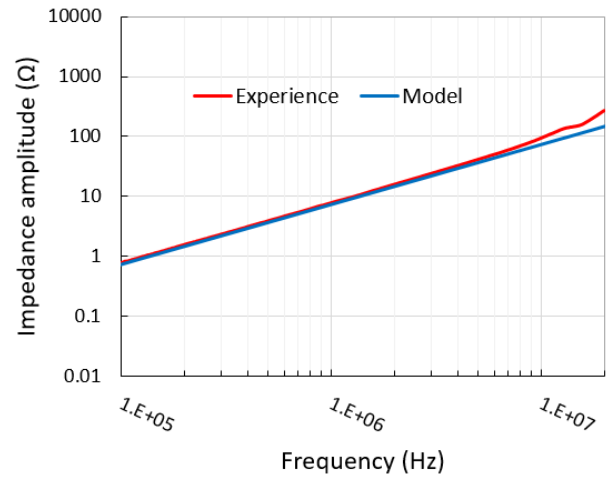
model. Another hypothesis to explain this offset may be due to the influence of the measurement circuit in these two configurations where the measurement cables are about 2 m long. The addition of an inductance in series with the measurement circuit could improve the response of these last two measurements. These two points will be discussed in the next section.

### B. RESULTS WITH MODEL IMPROVEMENT ELEMENTS

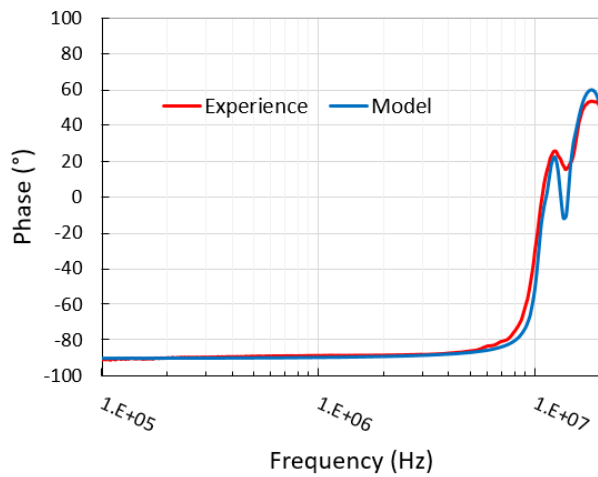
The addition of the equivalent circuit of the test tap as well as the equivalent series resistance to the model has made it possible to further improve its response, this is clearly observable in Figures 9 and 10 which present the impedance frequency analysis of configuration 1 and 2 respectively. Indeed, the resonance peaks in the frequency range from 10 MHz to 20 MHz has decreased thanks to the dumping effect caused by the series resistors. Now the response of the model



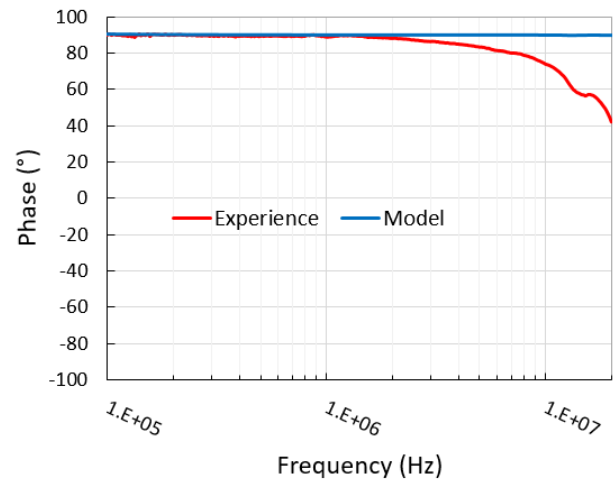
(a)



(a)



(b)



(b)

**FIGURE 10.** Impedance frequency analysis of the bushing using the configuration 2, with improvement elements. Model results in blue and experimental results in red. (a) amplitude measurement, (b) phase measurement.

has been greatly improved over the entire frequency range with a frequency response that has the same appearance as that of the impedance experimental measurements. However, it still has some deviation related to other modeling or measurement imperfections.

For the 3<sup>rd</sup> configuration, we discussed earlier that the offset could also be due to the measurement circuit which is essentially inductive (measuring cable), to compensate for this, an inductance of values  $10^{-7}$  H has been added in series. The latter is estimated from the measurements made on the cables used. These results presented in Figure 11 show that the addition of this inductance improves considerably the response of the model. The inductive behavior is still present, however, the resonance peaks that have been in the first version of the model disappeared further improving the response of the model. Indeed, the difference in amplitude

**FIGURE 11.** Impedance frequency analysis of the bushing using the configuration 3, with improvement elements. Model results in blue and experimental results in red. (a) amplitude measurement, (b) phase measurement.

between the model and the measurement has been compensated. Nevertheless, in terms of phase we have  $90^\circ$  in the whole frequency range, the addition of the inductance of the measurement circuit did not modify the shape of the phase.

## V. CONCLUSION

The aim of this work is to develop a model of high voltage bushings capable to simulate the bushing behavior till 20 MHz. This model will make it possible to study the behavior of bushings under fast and very fast transient overvoltages. To model such a system, the equivalent electrical circuit approach has been adopted. This approach of modeling has the advantage of reduced computing time and it provides access to the electrical quantities in each part of the bushing. To determine each element of the equivalent circuit, analytical

formulas have been used. A numerical simulation by COMSOL Multiphysics® has been also carried out in this work in order to check the validity of these equations over the studied frequency range.

The calculation of the model parameters as well as the modeling itself have been executed on Matlab/Simulink®. The main capacitor core of the bushing is composed of a central conductor, OIP insulation, and 41 aluminum layers. To characterize such a model, an impedance analysis has been performed over a wide range of frequencies, following the same configurations that were carried out in the experimental study.

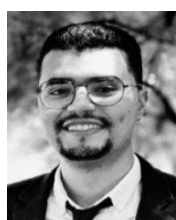
The model provides a response which is in a good agreement and accuracy compared to the experimental results of the impedance measurement. At the beginning, high frequency resonances were observed due to modeling imperfections and the assumptions made on the analytical equations. The model presented discrepancies in its frequency behavior between 10 and 20 MHz. Improvements have been proposed on the model by adding the equivalent electrical circuit of the test tap, the equivalent series resistances, as well as the inductance of the measurement circuit for the 3<sup>rd</sup> configuration. These modifications have largely improved the frequency response of the model.

The use of this model could make it possible to know the distribution of the electrical voltage and the electric field within a transformer bushing and thus to understand the mechanisms of failures and possibly to allow improvements of the structure to homogenize the distribution of the electric field. Moreover, this equivalent circuit model can be added to other transformer circuit models and transmission lines to investigate transients and high frequency response of a more complex system. For future works, in order to improve the accuracy of the model, the frequency effect on the circuit elements values has to be considered.

## REFERENCES

- [1] Y. Li, Y. Shang, L. Zhang, R. Shi, and W. Shi, "Analysis of very fast transient overvoltages (VFTO) from onsite measurements on 800 kV GIS," *IEEE Trans. Dielectr. Electr. Insul.*, vol. 19, no. 6, pp. 2102–2110, Dec. 2012, doi: 10.1109/TDEI.2012.6396970.
- [2] S. M. H. Hosseini, Z. Bagheri, and S. Darvishi-Niafenderi, "Modeling of 420 kV GIS Substation and Research on Very Fast Transient Overvoltage (VFTO)," *Res. J. Appl. Sci. Eng. Technol.*, vol. 5, no. 8, Art. no. 8, 2013, doi: 10.19026/rjaset.5.4711.
- [3] A. Shakeel, K.-H. Park, K.-Y. Shin, and B. Lee, "A Study of Fast Front Transients of an HVDC Mixed Transmission Line Exposed to Bipolar Lightning Strokes," *Energies*, vol. 14, no. 10, Art. no. 10, Jan. 2021, doi: 10.3390/en14102896.
- [4] H. I. Septyani, I. Arifianto, and A. P. Purnomoadi, "High voltage transformer bushing problems," in *Proceedings of the 2011 International Conference on Electrical Engineering and Informatics*, Jul. 2011, pp. 1–4, doi: 10.1109/ICEEL.2011.6021566.
- [5] M. Wang, A. J. Vandermaar, and K. D. Srivastava, "Review of condition assessment of power transformers in service," *IEEE Electr. Insul. Mag.*, vol. 18, no. 6, pp. 12–25, Nov. 2002, doi: 10.1109/MEI.2002.1161455.
- [6] K. Walczak and J. Gielniak, "Temperature Distribution in the Insulation System of Condenser-Type HV Bushing—Its Effect on Dielectric Response in the Frequency Domain," *Energies*, vol. 14, no. 13, Art. no. 13, Jan. 2021, doi: 10.3390/en14134016.
- [7] "Transformer bushing reliability," *e-cigre*, Apr. 01, 2019, [https://e-cigre.org/publication/ELT\\_303\\_3-transformer-bushing-reliability](https://e-cigre.org/publication/ELT_303_3-transformer-bushing-reliability) (accessed Apr. 09, 2023).
- [8] H. Tian *et al.*, "Research on the deterioration process of electrical contact structure inside the  $\pm 500$  kV converter transformer RIP bushings and its prediction strategy," *IET Gener. Transm. Distrib.*, vol. 13, no. 12, pp. 2391–2400, 2019, doi: 10.1049/iet-gtd.2019.0110.
- [9] L. Damião *et al.*, "Online Monitoring of Partial Discharges in Power Transformers Using Capacitive Coupling in the Tap of Condenser Bushings," *Energies*, vol. 13, no. 17, Art. no. 17, Jan. 2020, doi: 10.3390/en13174351.
- [10] M. Pompili and C. Mazzetti, "Partial discharge behavior in switching-surge-aged oil-paper capacitor bushing insulation," *IEEE Trans. Dielectr. Electr. Insul.*, vol. 9, no. 1, pp. 104–111, Feb. 2002, doi: 10.1109/94.983893.
- [11] Insulation co-ordination - Part 1: Definitions, principles and rules, IEC 60071-1, 2019.
- [12] A. Ardito, R. Iorio, G. Santagostino, and A. Porrino, "Accurate modeling of capacitively graded bushings for calculation of fast transient overvoltages in GIS," *IEEE Trans. Power Deliv.*, vol. 7, no. 3, pp. 1316–1327, Jul. 1992, doi: 10.1109/61.141849.
- [13] J. G. Rodrigues Filho, J. A. Teixeira, M. R. Sans, and M. L. Barreira Martinez, "Very fast transient overvoltage waveshapes in a 500-kV gas insulated switchgear setup," *IEEE Electr. Insul. Mag.*, vol. 32, no. 3, pp. 17–23, 2016, doi: 10.1109/MEI.2016.7527121.
- [14] L. Zhao, L. Ye, S. Wang, Y. Yang, P. Jiang, and X. Zou, "Research on Very Fast Transient overvoltage During Switching of Disconnecter in 550kV GIS," in *2018 IEEE 3rd International Conference on Integrated Circuits and Microsystems (ICIM)*, Nov. 2018, pp. 114–118, doi: 10.1109/ICAM.2018.8596673.
- [15] G.-M. Ma, C.-R. Li, J.-T. Quan, and J. Jiang, "Measurement of VFTO Based on the Transformer Bushing Sensor," *IEEE Trans. Power Deliv.*, vol. 26, no. 2, pp. 684–692, Apr. 2011, doi: 10.1109/TPWRD.2010.2042467.
- [16] M. M. Rao, T. P. Rao, S. S. T. Ram, and B. P. Singh, "Simulation of Capacitively Graded Bushing for Very Fast Transients Generated in a GIS during Switching Operations," *J. Electr. Eng. Technol.*, vol. 3, no. 1, pp. 36–42, 2008, doi: 10.5370/JEET.2008.3.1.036.
- [17] H. Tang, G. Wu, M. Chen, J. Deng, and X. Li, "Analysis and Disposal of Typical Breakdown Failure for Resin Impregnated Paper Bushing in the Valve Side of HVDC Converter Transformer," *Energies*, vol. 12, no. 22, Art. no. 22, Jan. 2019, doi: 10.3390/en12224303.
- [18] M. Asif, H.-Y. Lee, K.-H. Park, A. Shakeel, and B.-W. Lee, "Assessment of Overvoltage and Insulation Coordination in Mixed HVDC Transmission Lines Exposed to Lightning Strikes," *Energies*, vol. 12, no. 21, Art. no. 21, Jan. 2019, doi: 10.3390/en12214217.
- [19] G. Wang, H. Xiao, L. Xiao, Z. Zhang, and Z. Xu, "Electromechanical Transient Modeling and Control Strategy of Decentralized Hybrid HVDC Systems," *Energies*, vol. 12, no. 15, Art. no. 15, Jan. 2019, doi: 10.3390/en12152856.
- [20] A. S. Zalhaf, E. Zhao, Y. Han, P. Yang, A. H. Almaliki, and R. M. H. Aly, "Evaluation of the Transient Overvoltages of HVDC Transmission Lines Caused by Lightning Strikes," *Energies*, vol. 15, no. 4, Art. no. 4, Jan. 2022, doi: 10.3390/en15041452.
- [21] L. Jin, Y. Xue, B. Zhao, J. Chen, and W. Zhang, "Electric field calculation and insulation analysis of high voltage insulating bushing," in *2013 2nd International Conference on Electric Power Equipment - Switching Technology (ICEPE-ST)*, Oct. 2013, pp. 1–4, doi: 10.1109/ICEPE-ST.2013.6804314.
- [22] B. Du, H. Sun, J. Jiang, X. Kong, and W. Yang, "Temperature-dependent electric field distribution in  $\pm 800$  kV valve-side bushing insulation for a converter transformer," *High Volt.*, vol. 6, no. 1, pp. 106–115, 2021, doi: 10.1049/hve.2019.0385.
- [23] G. Xie, S. Shi, Q. Wang, P. Liu, and Z. Peng, "Simulation and experimental analysis of three-dimensional temperature distribution of  $\pm 400$ -kV converter transformer valve-side resin impregnated paper bushing under high current," *IET Gener. Transm. Distrib.*, vol. 16, no. 15, pp. 2989–3003, 2022, doi: 10.1049/gtd2.12491.

- [24] B. Jurisic, I. Uglesic, A. Xemard, and F. Paladian, "High frequency transformer model derived from limited information about the transformer geometry," *Int. J. Electr. Power Energy Syst.*, vol. 94, pp. 300–310, Jan. 2018, doi: 10.1016/j.ijepes.2017.07.017.
- [25] Y. Yoon, Y. Son, J. Cho, S. Jang, Y.-G. Kim, and S. Choi, "High-Frequency Modeling of a Three-Winding Power Transformer Using Sweep Frequency Response Analysis," *Energies*, vol. 14, no. 13, Art. no. 13, Jan. 2021, doi: 10.3390/en14134009.
- [26] R. Khalili Senobari, J. Sadeh, and H. Borsi, "Frequency response analysis (FRA) of transformers as a tool for fault detection and location: A review," *Electr. Power Syst. Res.*, vol. 155, pp. 172–183, Feb. 2018, doi: 10.1016/j.epr.2017.10.014.
- [27] S. Alsuhaibani, Y. Khan, A. Beroual, and N. H. Malik, "A Review of Frequency Response Analysis Methods for Power Transformer Diagnostics," *Energies*, vol. 9, no. 11, Art. no. 11, Nov. 2016, doi: 10.3390/en9110879.
- [28] Y. Liu *et al.*, "A study of the sweep frequency impedance method and its application in the detection of internal winding short circuit faults in power transformers," *IEEE Trans. Dielectr. Electr. Insul.*, vol. 22, no. 4, pp. 2046–2056, Aug. 2015, doi: 10.1109/TDEL.2015.004977.
- [29] S. Wang *et al.*, "An Experimental Study of the Sweep Frequency Impedance Method on the Winding Deformation of an Onsite Power Transformer," *Energies*, vol. 13, no. 14, Art. no. 14, Jan. 2020, doi: 10.3390/en13143511.
- [30] H. Meng *et al.*, "A transmission line model for high-frequency power line communication channel," in *Proceedings. International Conference on Power System Technology*, Oct. 2002, pp. 1290–1295 vol.2. doi: 10.1109/ICPST.2002.1047610.
- [31] K. L. Kaiser, *Electromagnetic Compatibility Handbook*. CRC Press, 2004.
- [32] V. G. Welsby, *The Theory and Design of Inductance Coils*. Macdonald, 1950.
- [33] P. T. Bartkowski and P. R. Berning, "Inductance Calculations of Variable Pitch Helical Inductors." Defense Technical Information Center, Fort Belvoir, VA, Jul. 2015. doi: 10.21236/ADA625194.
- [34] M. N. S. Khan, *Transient Voltage Distribution in Bushing*. 2020. Accessed: Apr. 09, 2023. [Online]. Available: <http://urn.kb.se/resolve?urn=urn:nbn:se:kth:diva-292753>
- [35] "Self Inductance and Mutual Inductance of a Single Conductor and a Homogenized Helical Coil," *COMSOL*. <https://www.comsol.com/model/self-inductance-and-mutual-inductance-of-a-single-conductor-and-a-homogenized-he-12687> (accessed Apr. 09, 2023).
- [36] S. A. Schelkunoff, "The electromagnetic theory of coaxial transmission lines and cylindrical shields," *Bell Syst. Tech. J.*, vol. 13, no. 4, pp. 532–579, Oct. 1934, doi: 10.1002/j.1538-7305.1934.tb00679.x.
- [37] R. Venkatesh and S. R. Kannan, "Diagnostic testing and condition monitoring of transformer bushings," in *Annual Report Conference on Electrical Insulation and Dielectric Phenomena*, Oct. 2002, pp. 882–886. doi: 10.1109/CEIDP.2002.1048936.
- [38] S. Yoon, C. W. Lee, and S. M. Oh, "Characterization of equivalent series resistance of electric double-layer capacitor electrodes using transient analysis," *J. Power Sources*, vol. 195, no. 13, pp. 4391–4399, Jul. 2010, doi: 10.1016/j.jpowsour.2010.01.086.
- [39] R. Vicentini, L. M. Da Silva, E. P. Cecilio Junior, T. A. Alves, W. G. Nunes, and H. Zanin, "How to Measure and Calculate Equivalent Series Resistance of Electric Double-Layer Capacitors," *Molecules*, vol. 24, no. 8, Art. no. 8, Jan. 2019, doi: 10.3390/molecules24081452.



**Anes MESSADI** received his "Ingénieur d'état" degree in power engineering from Ecole Nationale Polytechnique d'Oran (Algeria) in 2020 and his Master degree in electrical engineering from Université de Paris-Saclay and CentraleSupélec (France) in 2022. His research interests include electrical grids, renewable energy, electromagnetic transients, electromagnetic compatibility and power engineering.



**Ayyoub ZOUAGHI** received his "Ingénieur d'état" and Master degrees in power engineering from Ecole Nationale Polytechnique d'Alger (Algeria) in 2013 and his Ph.D. degree in electrical engineering from Université de Poitiers (France) in 2019. He is currently an Associate Professor within the Electric Engineering department of Ecole Centrale de Lyon (France). His teaching activities include power engineering, electromagnetism, high voltage engineering and dielectric materials.

He carries out his research within Ampère Laboratory. His research interests include high voltage engineering, electric discharge phenomena, dielectric materials, electromagnetic transients, non-thermal plasma, and applied electrostatics. He is author/co-author of several scientific papers in international peer-reviewed journals.



**Esseddik FERDJALLAH** received his engineering degree from Ecole Nationale Polytechnique d'Alger in Algeria in 2011 and his PhD in 2015 from Université de Nantes in France. He is currently a technical manager of high voltage laboratories of bushing manufacturing at Siemens Energy. He has started in high voltage business since 2012 as a PhD candidate at Nantes university working on insulation monitoring for tidal applications, then he joined Trench group in

2016 as development engineer where he worked on the electrical design of bushings and instrument transformers. Esseddik participated also to the development of new innovative insulation technologies, bushings monitoring solutions and sustainable process projects.



**Christian VOLLAIRE** received the master's and Ph.D. degrees in electrical engineering from the École Centrale de Lyon, France, in 1994 and 1997, respectively. In 1998, he joined the AMPERE Laboratory (CNRS 5005). From 2015 to 2020, he was the Deputy Director of the Ampère Laboratory. Since January 2021, he has been the Director of the Laboratory. He is currently a Full Professor at the École Centrale de Lyon, his teaching focuses on electrical engineering and power electronics. He is responsible for Ampère's

electromagnetic compatibility (EMC) activity. His research interest includes EMC of power systems and contactless energy transfer using high-frequency electromagnetic waves. He is a member of the reading committee of several international journals, a member of the International Congress Scientific Committee, and a scientific leader for numerous industrial and institutional contracts. From 2015 to 2020, he was Deputy Director of the Ampère Laboratory. Since 1st January 2021, he is the Director of the Laboratory.



**Olivier RICHER** received his Engineer and Master degrees from Ecole Polytechnique and ENSTA Paris in 1999 and 2001 respectively. He started his industrial carrier as a design engineer at Areva. He occupied after that Project Manager positions at Alstom Power and Alstom Hydro. Since 2014, he works for Trench France as a Head of Engineering, then as a Head of R&D department

where he manages a team of skilled professionals. He participated to the creation of several patents and product lines.



**Luiz Fernando de OLIVEIRA** was born in Blumenau-SC, Brazil, in 1988. He graduated in Electrical Engineering from the Regional University of Blumenau (FURB) in 2013 and has a Master's degree in Electrical Engineering from UFSC (GRUCAD) since 2018, currently studying for a doctorate in the same institution. He performed activities in the production and technical areas in transformer manufacturer WEG S/A, between 2009 and 2013 he worked directly

with electrical calculation and transformer design, from 2013 he began to carry out research and development activities. He works at Hitachi Energy Brasil Ltda. since 2022 as a global dry transformer specialist with a focus on renewables.



**Arnaud BRÉARD** received the M.S. degree from the University Denis Diderot Paris VII, France, in 2004, and the Ph.D. degree in physics from the Ecole SUPELEC, in 2007. Since 2011, he has been a Lecturer, then a Full Professor with the École Centrale de Lyon and a Researcher with the Ampère Laboratory (UMR CNRS 5005). His research interests include electromagnetic modeling, inverse problems, signal processing, antenna and radar experimentation, electromagnetic compatibility, and wireless electromagnetic transmission.